BUCKLE YAJ.96.B20.D1.28.BUCKLE-A - CU ZN SN PB - BYZANTINE

Artefact name Buckle Yaj.96.B20.D1.28.buckle-a

Authors Ahmad. Abu-Baker (Yarmouk University, None)

Url /artefacts/1648/

The object

Credit A.Abu-Baker.

Fig. 1: General view of the front face of buckle-a,

Description and visual observation

Description of the artefact A complete metallic garment buckle consisting of a frame, a bar and a prong. The buckle's surface is hetereogeously corroded and has green, blue-green, and red-brown corrosion products, with the presence of light yellow soil sediments (Fig. 1).

Type of artefact clothing element

Origin Khirbet Yajuz, Jordan

Recovering date Excavation 1996

Chronology category Byzantine

chronology tpq 600 A.D.

chronology taq 600 A.D.

Chronology comment	
Burial conditions / environment	Soil
Artefact location	The Archaeological Museum at the University of Jordan, Amman, Amman
Owner	Department of Antiquities of Jordan
Inv. number	Yaj.96.B20.D1.28.buckle-a
Recorded conservation data	N/A

Complementary information

None.

Study area(s)

Credit A.Abu-Baker.

Fig. 2: Location of study areas for XRF analysis (red circles) and the sampling area for cross-section (dashed line),

Binocular observation and representation of the corrosion structure

The schematic representation below gives an overview of the corrosion structure(s) encountered on the buckle from a first visual macroscopic observation:

Strata	Type of strata	Principle characteristics
S1	Soil	Light brown soil sediments intermixed with CP1
CP1	Corrosion product	White corrosion spots
CP2	Corrosion product	Olive-green corrosion layer
CP3	Corrosion product	Black corrosion layer
CP4	Corrosion product	Turquoise-blue powdery corrosion products
CP5	Corrosion product	Blue corrosion product
CP6	Corrosion product	Red-brown corrosion product

M1	Metal	Yellow metal

Table 1: Description of the principal characteristics of the strata as observed under binocular and described according to Bertholon's method.

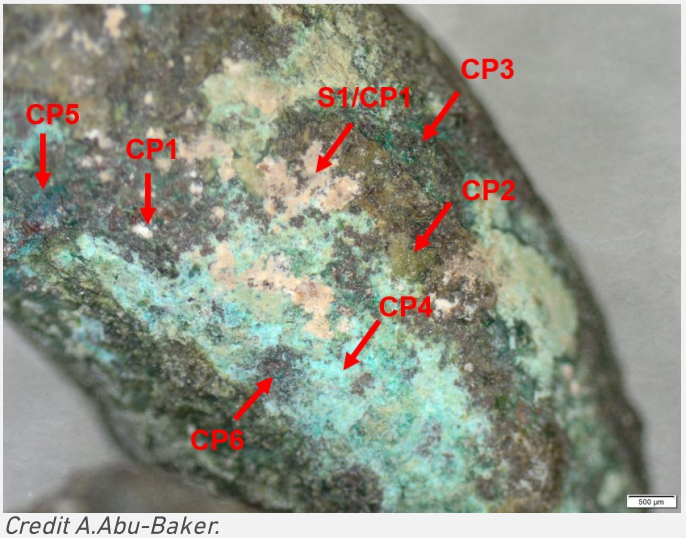

Credit A.Abu-Baker.

Fig. 3: Binocular observation of the surface deposit and corrosion products of buckle-a,

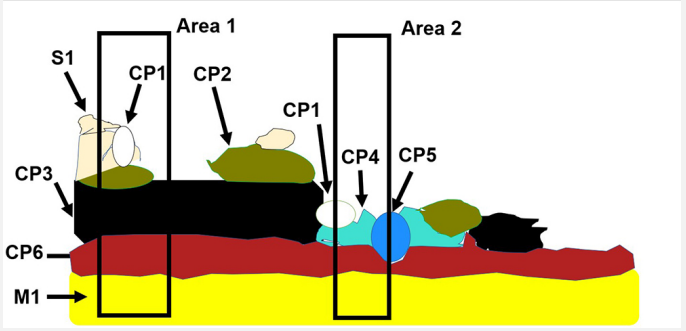

Credit A.Abu-Baker.

Fig. 4: Stratigraphic representation of the corrosion structure of buckle-a based on visual and binocular observations with indication of Areas 1 and 2 used to construct MiCorr stratigraphies Bi in Figs. 5 and 6,

MiCorr stratigraphy(ies) – Bi

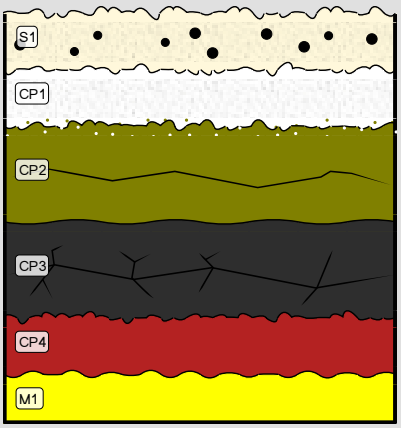

Fig. 5: Stratigraphic representation of the corrosion structure of buckle-a observed macroscopically under binocular microscope using the MiCorr application. The characteristics of the strata are only accessible by clicking on the drawing that redirects you to the search tool by stratigraphy representation. This representation can be compared to Fig. 4 considering that CP4 in Fig. 5 is CP6 in Fig. 4, credit A.Abu-Baker.

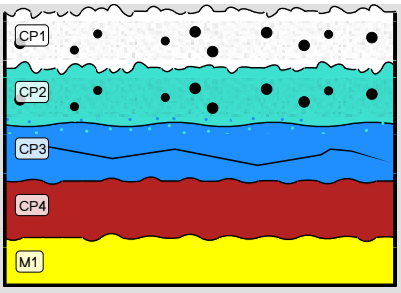

Fig. 6: Stratigraphic representation of the corrosion structure of buckle-a observed macroscopically under binocular microscope using the MiCorr application. The characteristics of the strata are only accessible by clicking on the drawing that redirects you to the search tool by stratigraphy representation. This representation can be compared to Fig. 4 considering that CP2, CP3 and CP4 in Fig. 6 are CP4, CP5 and CP6 respectively in Fig. 4, credit A.Abu-Baker.

Sample(s)

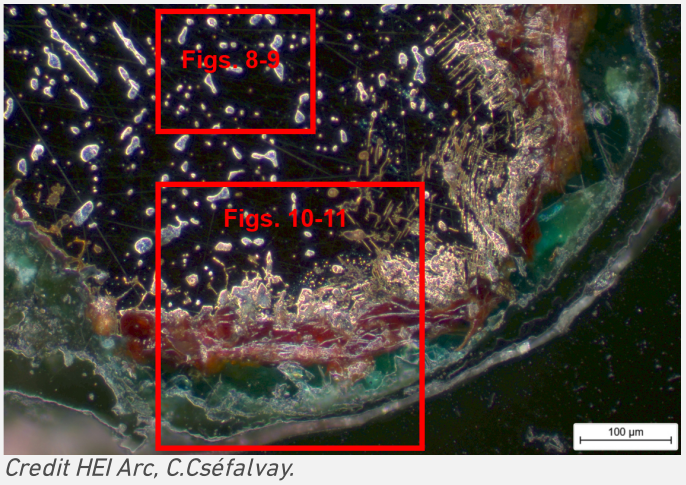

Credit HEI Arc, C.Céfalvay.

Fig. 7: Micrograph of the cross-section of the sample from Fig. 2 in dark field showing the locations of Figs. 8-9, 10-11,

Description of sample	A cross-section taken from the back-end of the prong of the buckle.
Alloy	Cu Zn Sn Pb
Technology	Cast
Lab number of sample	
Sample location	The Archaeological Museum at the University of Jordan, Amman, Amman
Responsible institution	The Archaeological Museum at the University of Jordan, Amman, Amman
Date and aim of sampling	May 2023. Sampling aimed to study the composition, corrosion, and microstructural properties of the artefact.

Complementary information

None.

Analyses and results

Analyses performed:

- **Non-Invasive approach**

XRF: with handheld portable X-ray fluorescence spectrometer (NITON XL3t 950 Air GOLDD+, Thermo Fischer®). General Metal mode, acquisition time 60s (filters: Li20/Lo20/M20).

- Invasive approach

- Metallography: The polished cross-section was observed by optical microscopy (OM) in bright and dark field modes using a Leica DM/LP polarizing light microscope. The OM in dark field mode allowed us to observe and quantify morphological, textural, microstructural and interfacial features of the strata. The cross-section was then etched with ammonium persulphate 10% in water to examine the microstructure using bright-field illumination, which helped to identify the manufacturing technique of the artifact.

- SEM-EDS: the sample was coated with a Pt layer and the analysis of the corrosion layers and internal alloy was performed using a SEM-FEG JEOL 7001-F equipped with a silicon-drift EDS Oxford detector (Aztec analysis software) with an accelerating voltage of 20 kV and probe current at about 9 nA. The relative error is considered of about 10% for content range <1wt%, and 2% for content range of >1wt%.

- XRD: The mineralogical composition of the corrosion products of buckle-a was examined by X-ray diffraction (XRD) analysis using a Shimadzu LabX, XRD-6000 X-ray diffractometer. To minimize the amount of corrosion products taken for the analysis, a small amount was scratched off from the surface of the artifact, dispersed in ethanol, then spread on a microscopic glass slide, the ethanol was allowed to dry off, then the glass slide covered with the thin layer of corrosion products powder was placed in the XRD instrument for analysis. The X-ray was generated from an anticathode copper (Cu) tube with a wavelength CuKα = 1.54178 A. The operation was at 40 kV and 30 mA, the 2θ analysis range was 5–80o, and the scan speed was 2o per minute.

Non invasive analysis

XRF analyses were carried out on the surface of buckle-a (Fig. 2). All strata (deposit, corrosion products and metal) were analyzed at the same time. Buckle-a is presumably a quaternary Cu-Zn-Sn-Pb alloy (leaded gun metal). The presence of P and Ca could be attributed to the hydrolysis of hydroxyapatite ($Ca_5(PO_4)_3OH$) from the skeletal materials in the neighboring bodies where the artifacts were excavated (Fan et al. 2020; Abu-Baker and Khalil 2022; Abu-Baker 2023b). The Si, Al, Fe are the elements of soil deposits (Rostoker et al. 1989).

Buckle a			
Element	buckle a.1	buckle a.2	buckle a.3
Cu	69	70	69
Zn	8	6	8
Pb	6.7	7.7	8.7
Sn	2.3	2.4	2.7
Si	11	13	7.6
P	0.7	0.5	2.3
Fe	0.2	0.3	0.3
Al	1.3	0	1.4

Table 2: Chemical composition of the surface of buckle-a analyzed by XRF at three representative points shown in Fig. 2.

Metal

The EDS analysis of the internal alloy of buckle-a showed that it is made from a quaternary Cu-Zn-Sn-Pb alloy. This result is in a good agreement with the non-invasive XRF analysis result.

Element	Wt. %
Cu	83
Zn	9
Sn	3
Pb	5

Table 3: EDS analysis of the internal alloy of buckle-a (Fig. 8).

The OM examination of the etched cross-sections of buckle-a revealed an as-cast dendritic microstructure (Fig. 9). The presence of cored dendrites and strain lines suggests that the artifact was cold-worked without annealing (Scott 1991: 7–8; Scott & Schwab 2019: 154). SEM micrograph (Fig. 8) shows the presence of air porosity and lead globules (in white).

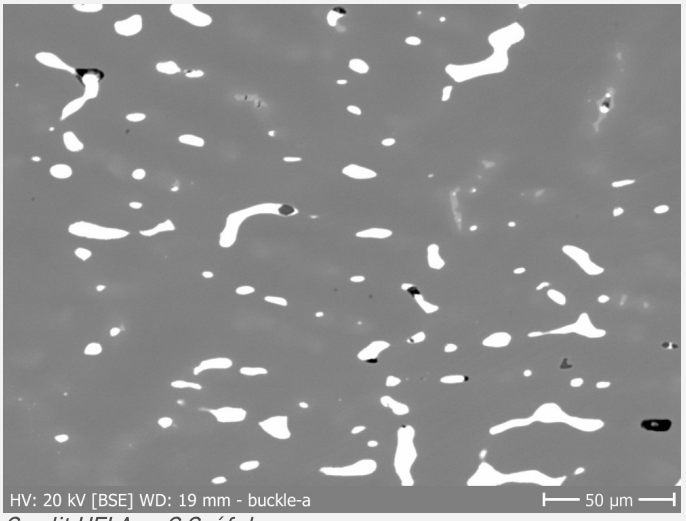

Credit HEI Arc, C.Cséfalvay.

Fig. 8: SEM image of the internal alloy of buckle-a. The dendritic structure appears in the background, while lead inclusions are in white,

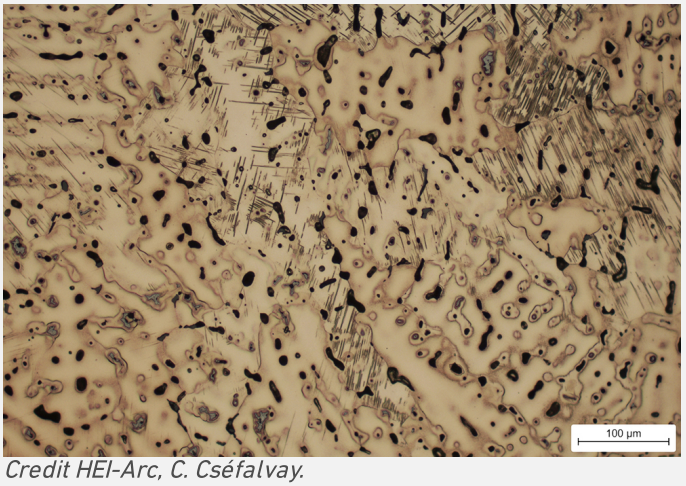

Credit HEI-Arc, C. Cséfalvay.

Fig. 9: OM image of the etched cross-section of buckle-a,

Microstructure	Dendritic structure with pores and inclusions
First metal element	Cu
Other metal elements	Zn, Sn, Pb

Complementary information

None.

Corrosion layers

The dark-field OM examination (Fig. 10) and EDS elemental mapping (Fig. 11) of the unetched cross-section of buckle-a showed depletion of zinc from areas in the corroded metal layer (CM1), i.e., CM1 is enriched with Pb and Cl while zinc is missing, indicating selective leaching of zinc from the alloy and the occurrence of dezincification. The external corrosion layer (CP1) showed the presence of Cu, Zn, Pb, C, O, P, and Cl, which could be attributed to the presence of corrosion products of copper, zinc, and lead (carbonates (malachite ($CuCO_3.Cu(OH)_2$) and smithsonite ($ZnCO_3$)), chlorides (atacamite (α-$Cu_2(OH)_3Cl$) and paratacamite (γ-$Cu_2(OH)_3Cl$) and phosphates (cornetite ($Cu_3(PO_4)(OH)_3$)) as indicated by the XRD analysis (Fig. 12). The Si, Al, and Ca in the soil (S1) and CP1 layers are the elements of soil deposits, i.e. aluminosilicate and calcite deposits. The second corrosion layer (CP2) layer showed mainly the presence of Cu and O, which could indicate a cuprous oxide corrosion layer (Cu_2O as indicated by XRD - Fig. 12). It should be noted that the presence of P and Ca in the CP1 layer could also indicate the effect of phosphate species released by the hydrolysis of hydroxyapatite ($Ca_5(PO_4)_3OH$) from the skeletal materials in the neighboring bodies buried in the cemetery where the buckles were excavated, which induced the formation of copper phosphate minerals (cornetite) (Fan et al. 2020; Abu-Baker and Khalil 2022; Abu-Baker 2023b). It seems that the formation of insoluble phosphate corrosion products on the surface of the artifact improved its stability, reduced the risk of activating the chloride-based corrosion, and suppressed the continuation of dezincification from the internal alloy in the uncontrolled environment of the storage area. The original surface has been preserved and corresponds to the interface between CP1 and CP2, i.e., at the top of the cuprite layer (Bertholon 2001). The white spots appearing in the internal sound metal (M1) of buckle-a are the lead globules. The high concentration of Pb below CP1 and below CP2 in buckle-a as observed in the elemental mapping image is probably attributed to the diffusion of Pb towards the exterior of the object during burial and corrosion processes and the manufacturing technique in which the artifact was cast in a mold where it was allowed to slowly cool, and due to gravity segregation, Pb pooled at the bottom of the mold and solidified in the external part of the alloy. In addition, leaching of the soluble zinc corrosion products from the CM1 zone made it enriched with lead or lead chlorides (Scott 2011; Abu-Baker and Khalil 2022; Abu-Baker 2023a; Abu-Baker 2023b). The presence of atacamite/paratacamite and the absence of nantokite (CuCl) in the XRD results suggest that the initially formed nantokite in the burial soil underwent oxidative hydrolysis, which induced the formation of atacamite/paratacamite under the uncontrolled storage conditions. The artifact has either been stabilized by this reaction or is in a metastable state if nantokite is present deeper in the alloy such that it was not collected in the samples obtained for XRD analysis (Scott 1990). The diffused zinc from the alloy reacted with the corrosive burial soil and after a prolonged exposure formed zincite and smithsonite.

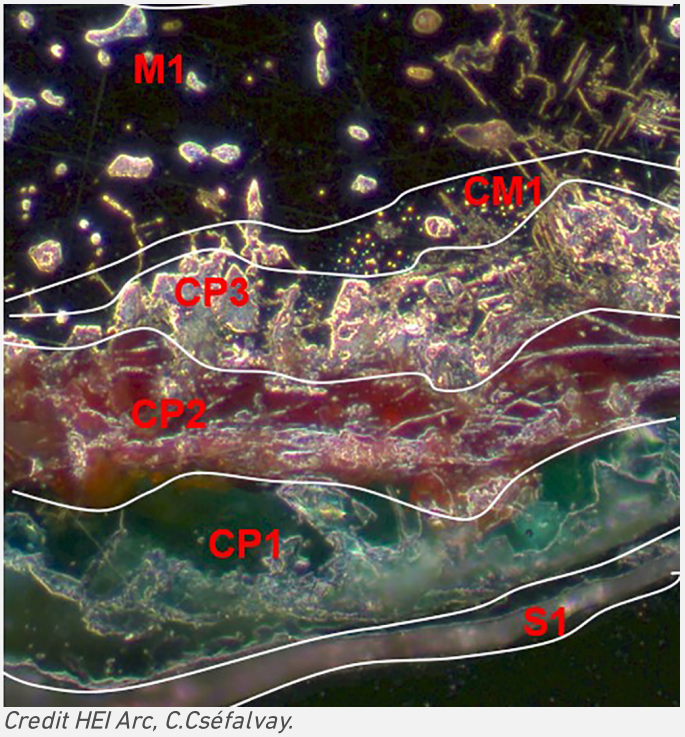

Credit HEI Arc, C.Cséfalvay.

Fig. 10: OM micrograph of the corrosion structure of the sample from Fig. 7 (detail), unetched, dark field. The strata S1 to M1 are indicated and also shown in the digital stratigraphy in Fig. 13,

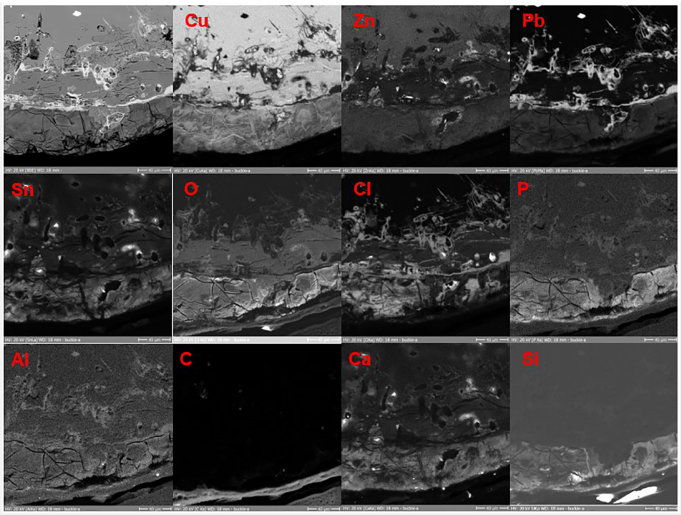

Credit HEI Arc, C.Cséfalvay.

Fig. 11: SEM image, BSE-mode, and elemental chemical distribution of the selected area (Fig. 10, detail),

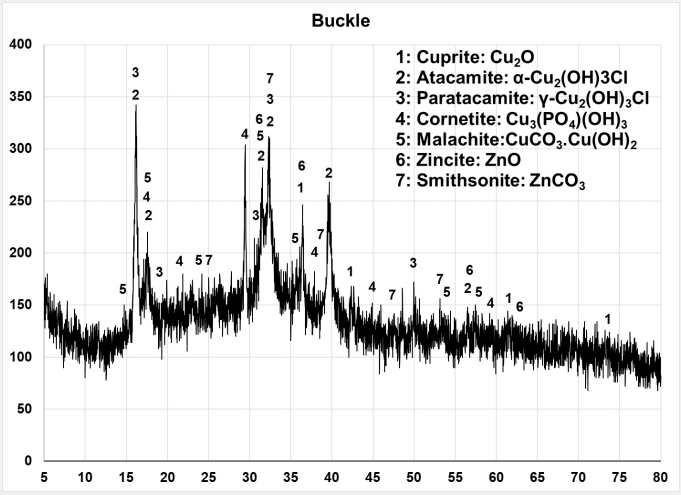

Credit A.Abu-Baker.

Fig. 12: XRD analysis of the corrosion products of buckle-a,

Corrosion form	Multiform - selective
Corrosion type	Dezincification

Complementary information

None.

MiCorr stratigraphy(ies) – CS

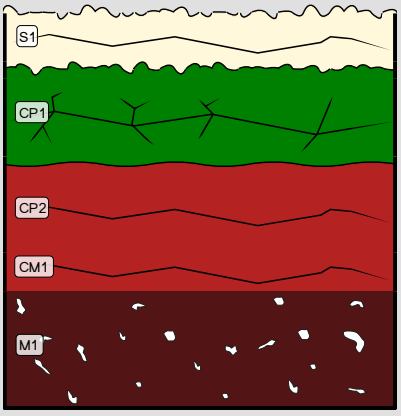

Fig. 13: Stratigraphic representation of the sample from buckle-a in cross-section (dark field) using the MiCorr application. The characteristics of the strata are only accessible by clicking on the drawing that redirects you to the search tool by stratigraphy representation. This representation was build according to Fig. 10, credit A.Abu-Baker.

Synthesis of the binocular / cross-section examination of the corrosion structure

The observation under binocular microscope of the whole artifact led to two different representative stratigraphies (Areas 1 and 2, Fig. 4). The cross-section obtained on a discreet area of the metal surface identified 2 CPs and a CM. With binocular microscope, it is possible to differentiate strata according to texture and light color changes that do not always correspond to significant changes in chemical composition, thus leading to a regrouping of several strata into one in the cross-section observation and physicochemical characterization.

The S1 and CP1 strata under binocular microscope of Area 1 could be grouped and correspond to S1 in cross-section. The CP1 stratum in Area 2 corresponds to S1 in cross-section. CP2 of Area 1 or CP2 and CP3 of Area 2 under the binocular microscope could be grouped and correspond to CP1 in cross-section. Similarly, the CP3 and CP4 of Area 1 or CP4 of Area 2 under binocular microscope probably correspond to CP2 in cross-section. The corroded metal (CM) zone lies between the external corrosion product (CP) zone and the sound metal (M). It is characterized by corrosion that has developed within the metal while preserving remnants of the original metallic structure, i.e., the dezincified copper-rich network, and can therefore only be observed on a cross-section.

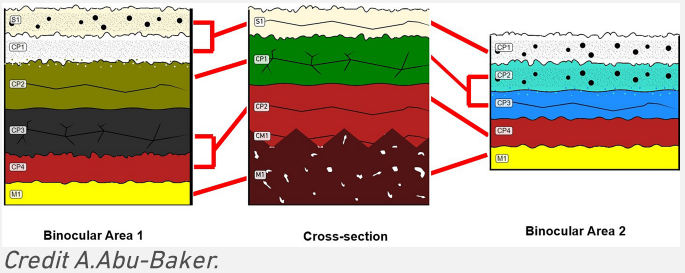

Credit A.Abu-Baker.

Fig. 14: Stratigraphic representation side by side of binocular views and cross-section (dark field) of buckle-a,

Conclusion

Buckle Yaj.96.B20.D1.28.buckle-a is a quaternary alloy of Cu-Zn-Sn-Pb with Zn as the highest alloying element (8-9 wt%). The presence of cored dendrites and strain lines in its microstructure suggests that the cast alloy was cold-worked without annealing. After observation of the corrosion structure in cross-section, it is possible to identify the original surface of the buckle that has been preserved and corresponds to the interface between CP1 and CP2. As for the corrosion structure underneath, it presents the phenomenon of dezincification commonly observed in brasses, i.e. a selective leaching of the more active metal, zinc, from the alloy. The elemental distribution of Cu and Zn in the EDS maps show patterns of depletion across the alloy. Corrosion products seem to be typical of copper-based alloys. The insoluble phosphate corrosion products on the surface of the artifact improved its stability against dezincification and active chloride-based corrosion present in the internal pits. The investigation of the internal corrosion was complementary to that of external corrosion and helped provide complete information about the corrosion of this artefact, which allowed corrosion stratigraphy representations to be created using the MiCorr modeling program.

References

References on objects

Khalil, L.(1998) University of Jordan excavations at Khirbat Yajuz. Annu. Dep. Antiq. Jordan (ADAJ) 42, 457–472.

References on analytical methods and interpretation

1. Abu-Baker, A.N. (2023a) Analytical investigation and electrochemical conservation treatment for archaeological copper alloy artifacts from Jordan. Conserv. Patrim. 42, 38–55.
2. Abu-Baker, A.N. (2023b) A technical examination of the corrosion and microstructural features of copper alloy artifacts from the Byzantine period at Khirbet Yajuz, Jordan. Metallogr. Microstruct. Anal. 12, 276–288.
3. Abu-Baker, A.N., Khalil, L.A. (2022) An analytical study of the corrosion behavior and microstructural

properties of a group of copper alloy artifacts from the Khirbet Yajuz archaeological site, Jordan. In: Mardikian, P., Näsänen, L., Arponen, A. (eds.) Metal 2022: Proceedings of the Interim Meeting of the ICOM-CC Metals Working Group, pp. 221–230. International Council of Museums – Committee for Conservation (ICOM-CC) and The National Museum of Finland, Helsinki.
4. Abu-Baker, A.N., Khalil, L.A., Gonmeen, T. (2021) A multi-analytical exploration of the chemical composition, microstructural properties and corrosion inhibiting treatment for an archaeological brass censer from Umm Zuwaytinah, Amman. Nucl. Instrum. Methods Phys. Res. B 502, 73–79.
5. Bertholon, R. (2000) La limite de la surface d'origine des objets métalliques archéologiques, caractérisation, localisation et approche des mécanismes de conservation (The Limit of the Original Surface of Archaeological Metal Objects: Characterization, Location and Approach to Conservation Mechanisms), in French. Ph.D. Dissertation, University Paris 1 Panthéon-Sorbonne, France.
6. Bertholon, R. (2001) Characterization and location of the original surface of corroded archaeological objects. Surf. Eng. 17(3), 241–245.
7. Degrigny, C., Dillmann, P., Gaspoz, C., Neff, D. (2022) Exploitation and dissemination of MiCorr as a diagnostic support tool for heritage metals. Conserv. 360° 2, 459.
8. Degrigny, C., Gutknecht, N., Valbi, V., Neff, D., Dillmann, P., Berranger, M., Gaspoz, C., Letourmy, B. (2025) Transdisciplinary collaboration for the multi-scale description of corrosion structures in metallic heritage. In: Neff, D., Grassini, S., Watkinson, D., Emmerson, N. (eds.) Bridging the Gap: Corrosion Science for Heritage Contexts, EFC Series, vol. 73, pp. 147–163. Woodhead Publishing in Materials, Cambridge.
9. Eary, L.E. (1999) Geochemical and equilibrium trends in mine pit lakes. Appl. Geochem. 14(8), 963–987.
10. Fan, X., Wang, Q., Wang, Y. (2020) Non-destructive in situ Raman spectroscopic investigation of corrosion products on the bronze dagger-axes from Yujiaba site in Chongqing, China. Archaeol. Anthropol. Sci.
11. Graziani, V., Iorio, M., Albini, M., Riccucci, C., Di Carlo, G., Branchini, P., Tortora, L. (2020) Metals and environment: chemical outputs from the interaction between gilded copper-based objects and burial soil. Front. Mater. 7, 32.
12. Rostoker, W., Pigott, V.C., Dvorak, J.R. (1989) Direct reduction to copper metal by oxide–sulfide mineral interaction. Archeomaterials 3(1), 69–87.
13. Scott, D.A. (1990) Bronze disease: a review of some chemical problems and the role of relative humidity. J. Am. Inst. Conserv. 29(2), 193–206.
14. Scott, D.A., Schwab, R.(2019) Metallography in Archaeology and Art, p. 154. Springer, Cham.